JOURNAL OF GEOPHYSICAL RESEARCH, VOL. 106, NO. A11, PAGES 24,733–24,744, NOVEMBER 1, 2001

An investigation into the influence of tidal forcing on F region equatorial vertical ion drift using a global ionosphere-thermosphere model with coupled electrodynamics

G. H. Millward,[1] I. C. F. Müller-Wodarg,[1] A. D. Aylward,[1]
T. J. Fuller-Rowell,[2] A. D. Richmond,[3] and R. J. Moffett[4]

Abstract.
A recent development of the coupled thermosphere-ionosphere-plasmasphere model (CTIP) has been the inclusion of the electrodynamic coupling between the equatorial ionosphere and thermosphere. The vertical ion drifts which result are shown to be largely in agreement with empirical data, on the basis of measurements made at the Jicamarca radar and other equatorial sites [*Scherliess and Fejer*, 1999]. Of particular importance, the CTIP model clearly reproduces the "prereversal enhancement" in vertical ion drift, a key feature of the observational data. Inacurracies in the modeled daytime upward ion motion have been investigated with regard to changing the magnitude and phase of components of the lower thermospheric tidal forcing. The results show that daytime vertical ion motion is highly dependent upon both the magnitude and phase of the semidiurnal tidal component. In addition, the CTIP model shows the prereversal enhancement to be unaffected by changes in tidal forcing, but only for conditions of high solar activity. During periods of low solar activity the form of the prereversal enhancement is clearly dependant upon the magnitude and phase of the semidiurnal tide.

1. Introduction

The structure of the Earth's equatorial ionosphere results from a complex interaction between ionospheric conductivities, thermospheric winds, and the magnetic field, with the horizontal nature of the latter of key importance. One of the most important mechanisms at work is due to an ionospheric wind dynamo [*Rishbeth*, 1971a, 1971b, 1981]. The ionospheric wind dynamo operates when upper atmospheric winds move the electrically conducting medium through the Earth's magnetic field. The ions and electrons respond differently to the imposed wind, owing to a large difference in the ratio of gyrofrequency to collision frequency with neutral particles for the respective constituents [*Rishbeth and Garriot*, 1969]. The different ion and electron motions lead to an electromotive force that drives currents and causes electric polarization charges and electric fields to develop. In particular, the unique geometry at the equator leads to electric fields which drive the ions vertically, upward during the day and downward at night. The daytime vertical velocity leads to a "fountain effect" [*Hanson and Moffett*, 1966], with ions moving upward under this $\mathbf{E}\times\mathbf{B}$ drift and then downward and outward under the effect of gravity. The result is a daytime ionosphere which exhibits a characteristic minimum in electron density at the magnetic equator, with accompanying maxima located roughly 15°on either side. This is known as the "equatorial ionization anomaly" or "Appleton anomaly" [after *Appleton*, 1946]. In addition, physical conditions around sunset conspire to produce a marked "prereversal enhancement" in the vertical **ExB** drift [*Woodman*, 1970], which leads to very small equatorial ion densities and also to enhanced zonal thermospheric winds because of the large reduction in drag from the ionosphere.

The electrodynamic effects of horizontal equatorial winds have been assessed using a variety of two-dimensional electric potential models [e.g., *Tarpley*, 1970; *Heelis et al.*, 1974; *Richmond et al.*; 1976, *Eccles*, 1998a, 1998b]. Such models rely on the assumption that the

[1]Atmospheric Physics Laboratory, University College London, London, U.K.
[2]Cooperative Institute for Research in Environmental Sciences, University of Colorado/NOAA, Space Environment Center, Boulder, Colorado.
[3]High Altitude Observatory, National Center for Atmospheric Research, Boulder, Colorado.
[4]Upper Atmosphere Modelling Group, University of Sheffield, Sheffield, U.K.

Copyright 2001 by the American Geophysical Union.

Paper number 2000JA000342.
0148-0227/01/2000JA000342$09.00

conductivity in the magnetic field aligned direction, $\sigma_{\parallel}$, be assumed infinite [*Richmond et al.*, 1973a, 1973b] and thus magnetic field lines are equipotentials. This assumption allows for a fieldline integration of parameters, thus collapsing the three-dimensional equations onto a plane, without losing any of the physics of the system [*Takeda and Yamada*, 1987; *Haerendel et al.*, 1992; *Crain et al.*, 1993a,1993b; *Eccles*, 1998a,1998b].

Modeling work in this area has often utilized available parameterizations of ionospheric densities [e.g. *Bilitza*, 1990], and thermospheric compositions and winds [e.g., *Hedin*, 1991; *Hedin et al.*, 1991] in order to calculate the relevant fieldline integrated quantities [*Eccles*, 1998a, 1998b; *Du and Stening*, 1999a, 1999b]. Such approaches have proved extremely fruitful in determining the important processes at work but inevitably do not allow for any feedback between the ion densities, winds, and electric fields. Of recent, sophisticated three-dimensional global models of the coupled ionosphere-thermosphere system have allowed the possibility of calculating the mutual coupling among neutral dynamics, plasma dynamics, and the electric currents and fields [*Namgaladze et al.*, 1991; *Richmond et al.*, 1992; *Fesen et al.*, 2000]. The latest version of the coupled thermosphere-ionosphere-plasmasphere model (CTIP), described in section 2, calculates the electrodynamics in this fully coupled manner by using a description of the equatorial electrodynamics as given by *Richmond and Roble* [1987].

2. CTIP Model: History

The CTIP model is the concise name given to a nonlinear, coupled thermosphere-ionosphere-plasmasphere model. The model consists of four distinct components which run concurrently and are fully coupled with respect to energy, momentum, and continuity. The program incorporates (1) a global thermosphere model, (2) a high-latitude ionosphere model, (3) a mid and low-latitude ionosphere/plasmasphere model, and (4) a model of the electrodynamic coupling between the ionosphere and thermosphere at low latitudes, which is the subject here.

The thermospheric model was described originally by *Fuller-Rowell and Rees* [1980] and, more fully, in the Ph.D. thesis of *Fuller-Rowell* [1981]. At that stage, ionospheric densities were taken from an empirical ionospheric model [*Chiu*, 1975]. Subsequent work was concerned with developing a consistent description of the conservation of mean molecular mass for a two-constituent thermosphere [*Fuller-Rowell and Rees*, 1983], which had been absent from earlier model versions. The limitation imposed by using an empirical ionospheric model in describing dynamic conditions at high latitudes was removed by inclusion of a fully dynamic ionospheric model [*Quegan et al.*, 1982; *Fuller-Rowell et al.*, 1987]. At this stage the new, dynamic ionosphere was limited to high and mid latitudes, with the empirical model of *Chiu* [1975] still used for low latitudes. Subsequently, the model was further enhanced to include a fully dynamic model of the mid- and low-latitude ionosphere and plasmasphere [*Millward*, 1993] in the process finally becoming CTIP. Full descriptions of the thermospheric and high-latitude ionospheric models and the plasmaspheric extension have been given by *Fuller-Rowell et al.* [1996], and *Millward et al.* [1996], respectively.

3. Recent Developments

Of recent, there have been a number of significant developments made to CTIP which make the model considerably different from that which was fully documented by *Millward et al.* [1996]. Two major changes have occurred within the structure of the mid- to low-latitude ionosphere/plasmasphere component.

3.1. Model Resolution

First, for a given magnetic longitude the number of independent flux tubes solved concurrently has been increased from 15 to 70. Each of the 70 flux tubes are spaced in L shell (or equatorial crossing height) such that the outer most tube lies at around L=3.5, while the inner most has an equatorial crossing height of 200 km. The 70 "L shell" tubes are repeated at 20 consecutive magnetic longitudes (with a spatial resolution of 18°) yielding a total of 1400 flux tubes. The main reason for introducing a large increase in the number of flux-tubes is due to the fact that previously in CTIP the essential features of the low-latitude ionosphere, such as the equatorial ionisation anomaly, were not adequately well resolved. At lower altitudes the molecular ions NO^+ and O_2^+ are calculated with assumptions of photochemical equilibrium and at resolutions of 2°in latitude and 5°in longitude (rather than the previous 18°in longitude). The increase in longitudinal resolution for the molecuar ions, to be the same as used for the electrodynamics solver (described in section 3.4), was found to be necessary in order for the model to consistently reproduce the prereversal enhancement in the equatorial vertical velocity.

3.2. Reference Frames

The version of CTIP documented by *Millward et al.* [1996] solved the relevant ionospheric equations along flux tubes which were moving under the influence of a vertical **ExB** drift (and thus getting larger and smaller as time progressed). This Lagrangian framework required complex interpolation in order for parameters to be passed from, and to, the neutral thermospheric component of the code. In addition, the values of **ExB** drift had to be adjusted to ensure that each flux tube returned to its original starting point during a 24 hour simulation. Without such an imposition a number of consecutive CTIP runs would gradually inherit a low-

latitude ionosphere in which the flux tubes were increasingly disorganized. In addition, it was clear that for a more dynamic system involving coupled electrodynamics, and for which the **ExB** drift cannot be known in advance, this Langrangian frame of reference was unsuitable. For these reasons it was decided to change the low-latitude ionosphere/plasmasphere code to allow the equations to be solved in a fixed, Eulerian frame of reference. In this new system the flux tubes remain fixed, with the effects of motion due to **ExB** drifts incorporated via interpolation, a system which has always been used for the CTIP ionosphere at high latitudes.

3.3. Lower Thermospheric Tidal Forcing

Another recent major CTIP upgrade, relevant to the work presented here, has been the development of a new boundary to the lower thermospheric part of the code, to allow for the effects of lower thermospheric tidal forcing [*Müller-Wodarg*, 1997; *Müller-Wodarg et al.*, 2001]. (Note that the original version of the CTIP model did not allow for tidal forcing at the lower boundary of the model. The base pressure level within the model had a constant altitude (80 km) and temperature, and all wind components were set to zero.)

The analytical treatment of the tidal oscillations within CTIP comes from classical tidal theory [e.g., *Chapman and Lindzen*, 1970]. In essence, this linearized theory states that any given latitudinal profile of tidal amplitudes can be decomposed into Eigenfunctions called Hough modes. Oscillations are divided into two main categories; those that propagate vertically, allowing energy generated in the middle atmosphere to be carried up into the thermosphere, and those that are non propagating (or trapped). Within the CTIP model only the former are considered. The Hough modes are characterized by a pair of numbers (s,n), where s represents the longitudinal wave number and n represents the latitudinal wave number. Semi diurnal tides have a longitudinal wave number of 2 and are therefore represented by the family of $(2,n)$ modes. Similarly, the family of diurnal tides are represented as $(1,n)$ modes. Within CTIP the Hough modes used to calculate a global tidal pattern are the (1,1), (2,2), (2,3), (2,4), and (2,5) modes. Each mode is defined by an amplitude (in meters) and a local time of the maximum, as applied to the lower boundary pressure surface, for which the unperturbed height is 80 km. The amplitude is defined as the number that multiplies a given normalized Hough function. Thus a 200 m (2,2) mode means that the largest positive amplitude of the (2,2) mode will be 200 m, wherever this may be. The phase of a given component is then the local time at which this positive maximum value occurs. A tidal component with a maximum amplitude of 300 m at a local time of 0400 lt is denoted as 300, 4.0.

3.4. Modeling Electrodynamics

The CTIP model provides an ideal environment within which to understand equatorial electrodynamic coupling. The model of the Earth's electrodynamics, used for these studies, is taken from that described by *Richmond and Roble* [1987], and was also used in the studies of *Crain et al.* [1993a, 1993b]. Given the distributions of thermospheric winds and ionospheric conductivities (from the respective thermospheric and ionospheric components of the model), the electric fields and currents generated by the dynamo action can be calculated. Ohm's law is combined with the requirements of current continuity and electrostatic fields; that is,

$$\mathrm{J} = \sigma_P(\mathrm{E}_\perp + V_n \times \mathrm{B}) + \sigma_H b \times (\mathrm{E}_\perp + v_n \times \mathrm{B}) + \sigma_\parallel \mathrm{E}_\parallel b \quad (1)$$

$$\nabla \cdot \mathrm{J} = 0 \quad (2)$$

$$\mathrm{E} = -\nabla\Phi, \quad (3)$$

where J is current density, σ_P, σ_H, and $\sigma_\parallel$ are the Pederson, Hall, and parallel conductivities, respectively, $\mathrm{E}_\perp$ and $\mathrm{E}_\parallel$ are the electric field components perpendicular and parallel to the magnetic field B, and v_n is the neutral wind. This leads to a partial differential equation in Φ:

$$\nabla[\sigma_P(\nabla\Phi)_\perp + \sigma_H b \times \nabla\Phi + \sigma_\parallel(\nabla\Phi)_\parallel] = \nabla \cdot [\sigma_P \mathrm{V_n} \times \mathrm{B} + \sigma_H b \times (\mathrm{V_n} \times \mathrm{B})]. \quad (4)$$

This equation can be greatly simplified by assuming that field lines are equipotentials (i.e., Φ is constant along a field line) and that $\sigma_\parallel$ is infinite ($\mathrm{E}_\parallel = 0$). The partial diffential equation for Φ can then be reduced from three to two dimensions by integrating along field lines from their base in the Southern Hemisphere, through the equator, to the base in the Northern Hemisphere. The equation is solved subject to appropriate boundary conditions at the base of the ionosphere (i.e., $\mathrm{J}_\parallel = 0$, since ionospheric conductivity diminishes to zero below 100 km), to yield a global, two-dimensional potential, Φ. Electric fields in the magnetic zonal and vertical/meridional directions are then deduced (from equation (3)) yielding **ExB** ion drifts in the vertical and zonal directions, respectively. These ion drifts are then fed back into the ionospheric code and the whole coupled ionosphere-thermosphere system is recomputed. At present, the electrodynamics are computed for a simplified model of the Earth's magnetic field, a centerd tilted dipole, in which the magnetic field is considered to be dipolar, with an axis which intersects with the Earth's rotational axis at the center of the Earth, and with equal offsets, from the spin axis, in each hemisphere.

4. Model Runs

For our initial electrodynamic studies the CTIP model was run for equinox, June solstice, and December solstice conditions, each at high and low solar activity ($F10.7$ = 180 and 80, respectively), a total of six runs. In each simulation the model was run for 10 days (model time) under steady state conditions to allow the system to attain equilibrium. In all cases the lower thermo-

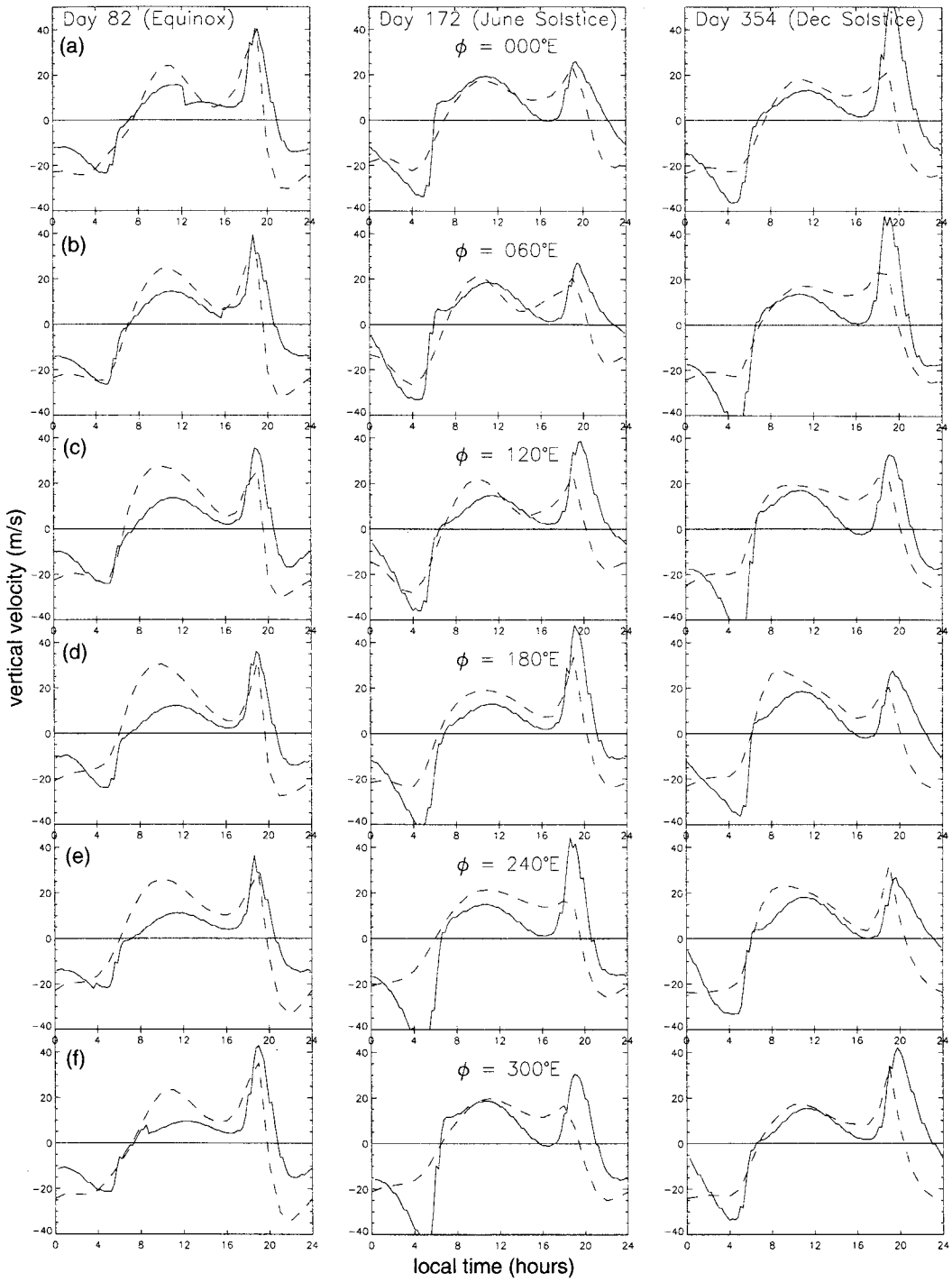

Figure 1. Equatorial vertical **ExB** drift velocity at 300 km, plotted against local time, for solar maximum conditions ($F10.7 = 180$) and with a solitary (2,2) tidal component of magnitude 300m and maximum at 0100 LT: results for equinox (left hand column), June solstice (middle column), and December solstice (right hand column), with the six rows showing geographic longitudes from 0°to 300°E (panels (a) to (f) respectively). In each panel the solid line shows results from CTIP, while the dashed line gives comparable results from the empirical model of *Scherliess and Fejer* [1999].

sphere was subjected to a solitary (2,2) tidal component of magnitude 300 m and a maximum at 0100 LT.

5. Results

Results from these simulations are shown in Figures 1 and 2. Figure 1 plots vertical **ExB** drifts at the magnetic equator, as a function of local time, at an altitude of 300 km and for conditions of high solar activity ($F10.7 = 180$). In all panels the solid line shows results from the CTIP model, with the dashed line showing results from the empirical model of *Scherliess and Fejer* [1999] for comparison. The three columns give results

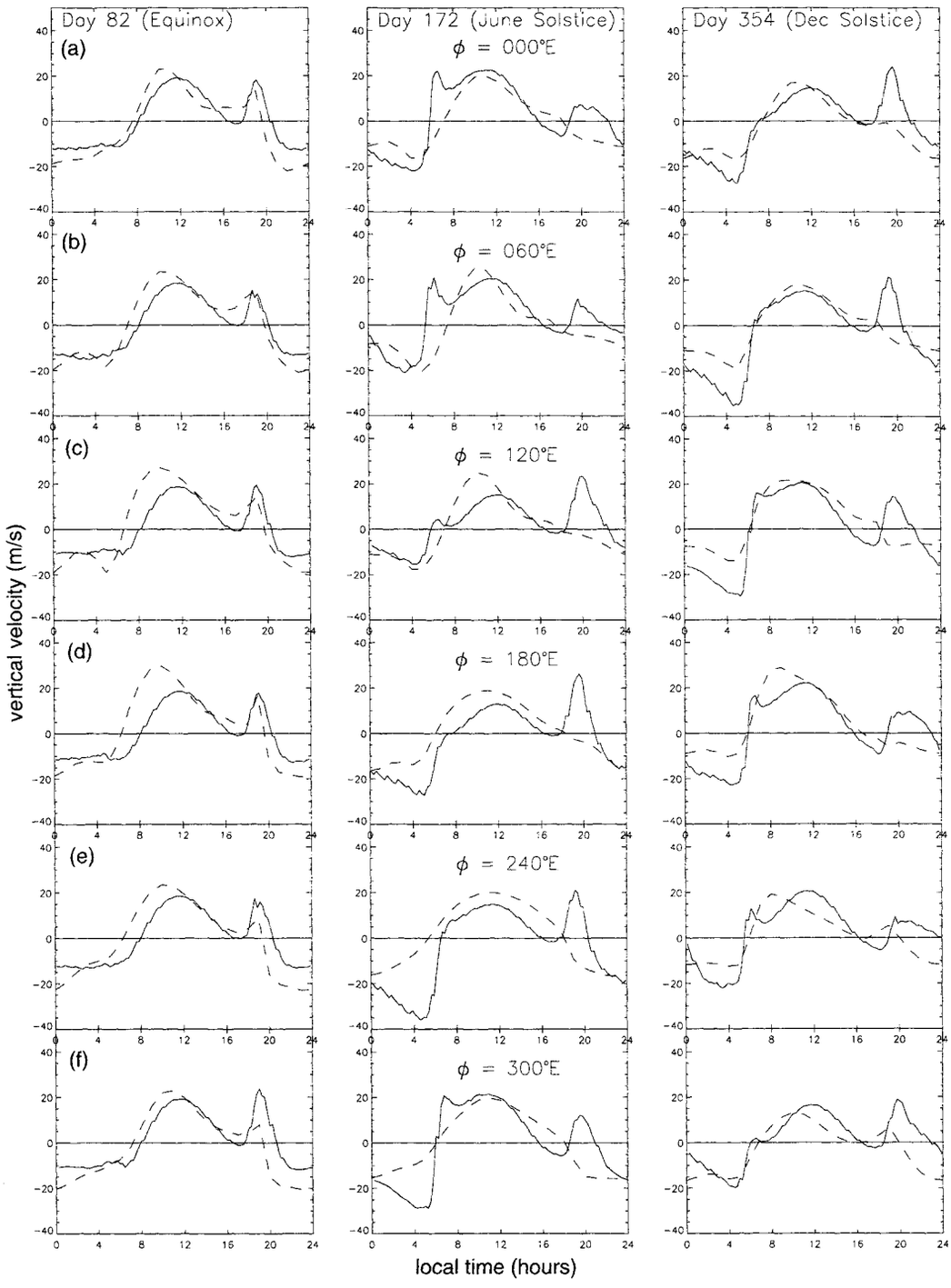

Figure 2. As for Figure 1, but for solar minimum conditions ($F10.7 = 80$).

for equinox (day 82), June solstice (day 172) and December solstice (day 354), respectively, while in each column the six rows show results for geographic longitudes from 0°to 300°E (denoted as (a) to (f)). Figure 2 is in exactly the same format as Figure 1, but for conditions of low solar activity ($F10.7 = 80$).

The CTIP results show much in common with the empirical data and also some important differences. For instance, in general, CTIP is modeling **ExB** drifts which are upward during the day and downward at night and are of a magnitude relatively close to those observed. The prereversal enhancement in upward **ExB** drift at around 1900 LT is clear in the CTIP results, though at times the values exceed those seen in the data. Also, the observed solar cycle dependence in the prereversal enhancement is reproduced clearly by CTIP. For instance, compare the results for equinox (left hand column) in Figure 1 with the same results in Figure 2. Here it is seen in both the data and the model results that the prereversal enhancement during high solar activity is much larger then during low solar activity. A similar statement can also be made for both June and De-

Table 1. Amplitudes (in metres) and phases (solar local time of maximum, in hours) for the five Hough modes used in the CTIP runs.

	(1,1)	(2,2)	(2,3)	(2,4)	(2,5)
Equinox	150,8.0	200,3.5	37,7.4	180,5.5	44,10.0
June	137,7.9	288,3.5	46,5.6	17,7.7	65,10.7
December	85,5.5	355,3.2	93,10.6	58,5.8	96,4.4

cember solstice results, though here the comparison is slightly spoiled by CTIP showing relatively large prereversal enhancements for low solar activity, whereas the data shows the prereversal enhancement to be largely absent for these conditions. Indeed it is of note that, in Figures 1 and 2, CTIP nowhere underestimates the prereversal enhancement, but sometimes overestimates it.

A second series of CTIP runs was undertaken, identical to those documented above (for which the results are shown in Figures 1 and 2), but utilising a more complete set of tidal modes. The amplitudes and phases of the Hough modes used in these simulations are given in Table 1. The semi diurnal values used are based on those given by *Forbes and Vial* [1989] whilst the diurnal values are based on results from the global scale wave model (*Hagan, private communication, Hagan et al.*, 1995; 1999). The same set of values were used for both high- and low solar activity runs.

Results from these simulations are given in Figure 3. Here the format is the same as in Figures 1 and 2, with vertical **ExB** drifts plotted against local time for CTIP simulations of equinox (left column), June solstice (center column), and December solstice (right column). The upper three panels (Figure 3a) show **ExB** results for a geographic longitude of 180°east at high solar activity. The lower panels (Figure 3b) are for low solar activity and the same longitude. As before the solid line shows the model results with the dashed line giving empirical data from *Scherliess and Fejer* [1999]. Thus the results in Figure 3a can be directly compared to Figure 1d and those in Figure 3b can be compared with Figure 2d. The comparison of Figure 3a with Figure 1d reveals that the prereversal enhancement is affected little by the form of the lower thermospheric tidal forcing, for high solar activity conditions. In contrast, a comparison of Figure 3b and Figure 2d reveals that for low solar activity conditions, the prereversal enhancement is clearly dependant upon the form of the tidal forcing.

An interesting feature of the CTIP results, not reproduced in the data, is the large upward "spike," a "postreversal enhancement" seen in the dawn sector around 0600 LT. The spike does not appear in the equinox results but is clear for both June and December solstice during low solar activity (e.g., Figures 2a and 2b at June solstice and Figure 3b for December solstice). Although it is clear that the "averaged" data of *Scherliess and Fejer* [1999] do not show any enhancement features around dawn, it is of note that studies of the vertical drift velocity for individual days sometimes do see such a feature. For instance, the winter solstice **ExB** drifts given by *Woodman* [1970], and reproduced by *Kelley*, [1989, Figure 3.3, p. 69] clearly show an occasional dawn enhancement feature of up to 40 m s^{-1}.

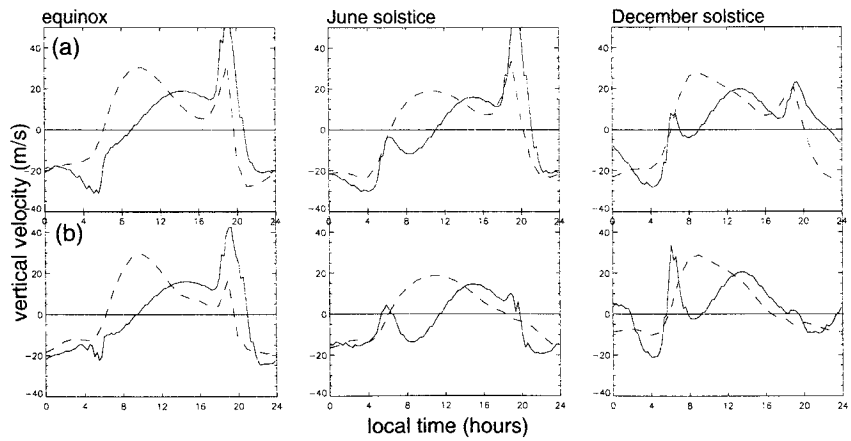

Figure 3. Equatorial vertical **ExB** drift velocity at 300 km and longitude 180 °east, plotted against local time. The tidal forcing used is as given in Table 1. Panel (a) shows results for solar maximum conditions ($F10.7 = 180$, equivalent to Figure 1d) whilst panel (b) shows results for solar minimum conditions ($F10.7 = 80$, equivalent to Figure 2d). The solid lines show results from CTIP, while the dashed lines are from the empirical model of *Scherliess and Fejer* [1999].

The same data show large variations in the morning sector **ExB** drifts for consecutive days. The point we are making here is that although the dawn spikes in many of the CTIP solstice results appear at odds with the results of *Scherliess and Fejer* [1999], there are examples for individual days in which such a feature is clearly seen.

5.1. Individual Tidal Components

Although the results given in Figures 1, 2, and 3 are extremely encouraging, it is apparent that the values of **ExB** drift during the morning period are not always well reproduced by CTIP. In addition, a comparison of the CTIP results in Figure 3 with those of Figures 1 and 2 shows that the values of **ExB** drift during the daytime are clearly influenced by the form of the tidal forcing. A clear avenue of investigation was therefore to look at the direct effect of the tidal forcing since it is known that winds in the lower thermosphere are an important factor in the daytime electrodynamics (via the so-called "E region dynamo").

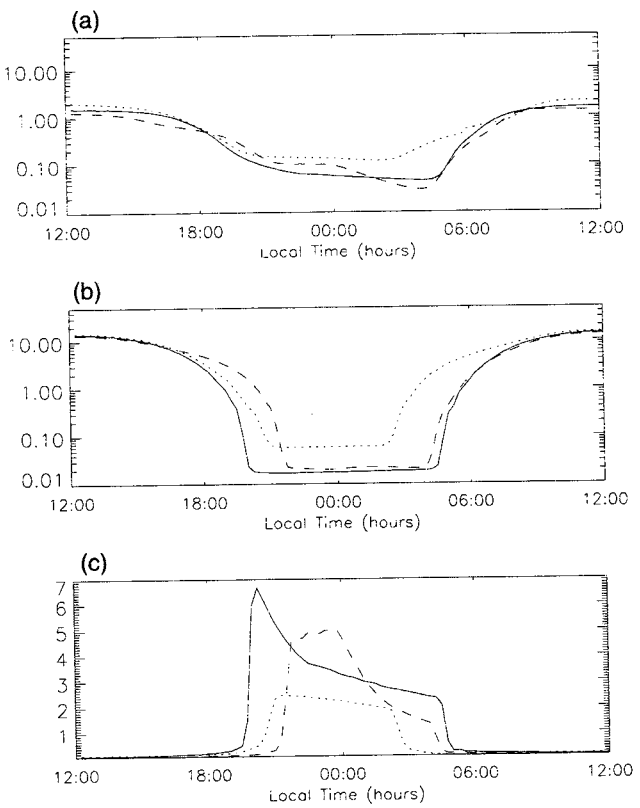

Figure 4. Field line integrated Pederson conductivity plotted against local time for a flux tube at 0°E geographic longitude and with an equatorial crossing height of 7500 km. Panel (a) shows the F region contribution to the integrated Pederson conductivity (mho), while panel (b) shows the E region contribution. Panel (c) gives the ratio of the F region contribution to E region contribution (no units). Results are for equinox (solid line), December solstice (dotted line), and June solstice (dashed line) and conditions of low solar activity ($F10.7$ = 80).

That the E region driven dynamo should dominate during the day, with the F region dominant at night, has been known for some time [i.e., *Rishbeth*, 1971a]. CTIP results of field line integrated Pederson conductivity, divided up into the contribution from the F region (defined as being above 160 km) and E region (80 - 160 km), are shown in Figures 4a and 4b, respectively). The results are for a flux tube with an equatorial crossing height of 7500 km and are for conditions of low solar activity ($F10.7$ = 80.). The three lines in each panel show results for equinox (solid line), December solstice (dotted line) and June solstice (dashed line). Figure 4c shows the ratio of the F region contribution to the E region contribution (i.e., Figure 4a / Figure 4b). Figure 4 shows clearly how the E region integrated conductivity dominates the F region during the daytime, by roughly a factor 10. During nighttime the E region conductivity drops sharply, the conductivity of the F region drops less sharply; thus the F region becomes dominant (by the factor demonstrated during nighttime in Figure 4c).

Clearly then, in examining any deficiencies in the CTIP-generated daytime vertical **ExB** drift we must look toward the form of the lower thermospheric (i.e., E region) winds, which are dominated by tidal forcing and, particularly, by the semidiurnal component.

A series of experiments were conducted in which CTIP was subjected to solitary tidal components with a variety of amplitudes and phases. Each simulation entailed starting from a CTIP run in which the system had established equilibrium with no tidal forcing (i.e., "tides off" run). The model was then run for a further 10 days in order to establish the new tidal component and allow the model to reach a new equilibrium, before outputting the relevant parameters.

First, we looked at the effect of applying a (2,2) tidal component to the model for equinox, solar maximum conditions. A variety of runs were conducted which utilized (2,2) tidal forcing with various magnitudes and phases.

Typical results are given in Figure 5. The Figure shows vertical **ExB** drifts at an altitude of 300 km and at the magnetic equator (geographic coordinates 10°S, 289°E). The vertical drifts are plotted against local time for four separate CTIP simulations. A fifth line (the dot-dot-dot-dashed line) gives equivalent results from the empirical model of *Scherliess and Fejer* [1999]. The solid line shows model results for a CTIP simulation with no tidal forcing. The line shows clearly how, in the absence of tidal forcing, the daytime vertical drifts are very small. The dotted line shows results from a CTIP run with a solitary (2,2) tidal component of magnitude 300 m and a maximum at 0400 LT. The dashed line shows results from another CTIP run with the (2,2) component of magnitude 300 m and maximum at 0100 LT. Similarly, the dot-dashed line shows a run with a (2,2) component of magnitude 600 m and maximum at 0100 LT. The results plotted in Figure 5 show that the semidiurnal wind variation in the lower thermosphere

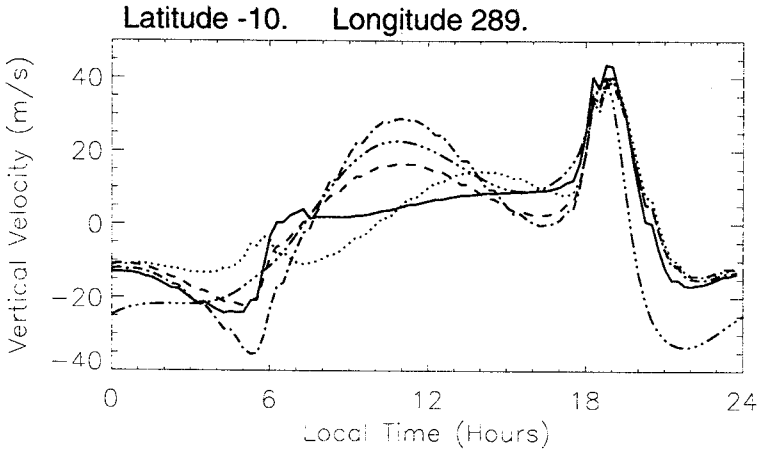

Figure 5. Vertical **ExB** drift velocity plotted against local time for equinox, solar maximum conditions. Four CTIP simulations are shown: "no tides" run (solid line), (2,2) tidal component of magnitude/LT 300 m/0400 (dotted line), (2,2) tidal component of magnitude/LT 300 m/0100 (dashed line), and (2,2) tidal component of magnitude/LT 600 m/0100 (dot-dashed line). Results from the empirical model of *Scherliess and Fejer* [1999] are shown for comparison (dot-dot-dot-dashed line).

plays a large role in the form taken by the daytime upward **ExB** drift and has a much smaller effect at night. They also do not appear to be a factor in determining the prereversal enhancement (at least not for solar maximum conditions), though they do appear to be important around dawn. Figure 6 shows values of NmF2 for a geographic longitude of 0°E and at 1300 LT, plotted against geographic latitude for the CTIP simulations detailed above in Figure 5. The four lines correspond to the four CTIP simulations, as described above for Figure 5; thus the four line styles correspond directly to the equivalent **ExB** results given in Figure 5. Figure 6 shows the effect of tidally generated vertical **ExB** drift on daytime equatorial F region ionospheric structure. The equatorial density minimum and corresponding maxima on either side are caused by a "fountain effect" in which plasma raised by an **ExB** drift is subsequently redistributed outward (to higher latitudes) and downward under the influence of gravity. Shown in this way it is clear that tidal forcing is directly responsible for creating the daytime "Appleton anomaly" feature in the equatorial ionosphere. It should be noted that from Figure 5, the differences in the values of vertical velocity for the separate runs are relatively small at 1300 LT (the local time of the results plotted in Figure 6). Much larger differences are seen at earlier local times (1000 to 1100 LT). This demonstrates how the equatorial electron density structure, the result of ambipolar diffusion, lags behind the applied vertical **ExB** drift by the order of an hour or so.

A further set of CTIP runs were undertaken to investigate the effect on the electrodynamics of the diurnal (1,1) tidal component. Three separate runs utilized a solitary diurnal (1,1) tidal component with an amplitude of 100 m and a maximum at 0600 LT, 0800 LT, and 1000 LT, respectively. The results are not plotted here but showed only very small deviations from the control tides off run. In other words, the simulations

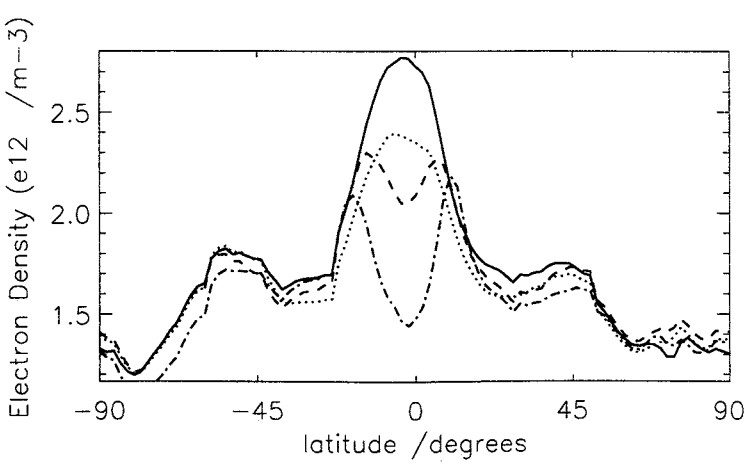

Figure 6. Peak electron density (NmF2) results plotted against latitude at 1300 LT, for the four CTIP simulations as documented in Figure 5.

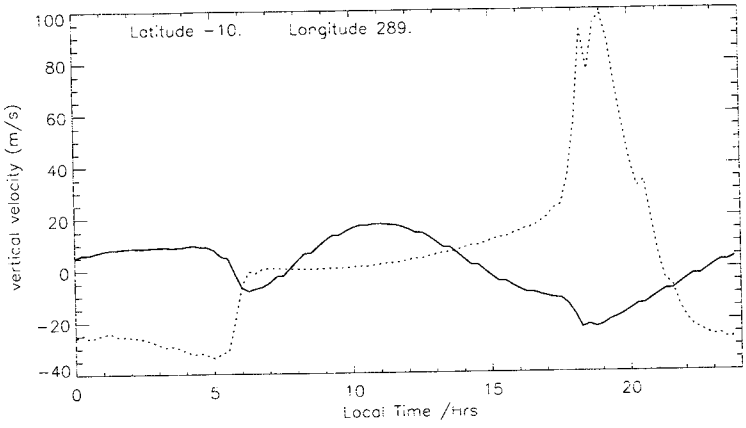

Figure 7. Vertical **ExB** drift velocity plotted against local time for equinox, solar maximum conditions. The solid line shows the vertical velocity produced by the "E region" dynamo. The dotted line is for the "F region" dynamo.

revealed the (1,1) diurnal tidal component to have little effect on equatorial electrodynamics.

5.2. Further Semidiurnal Experiments

To further establish the nature of the semidiurnal tidal control of daytime vertical ion drift, another two CTIP model runs were undertaken which utilized a solitary (2,2) tidal component (amplitude 300 m, maximum at 0100 LT) as input. For these simulations the thermospheric wind, as applied to the electrodynamics solver, was defined as being either "E region" (from 97 to 160 km) or "F region" (160 to 470 km), with the 160 km altitude separator being chosen to represent an average minimum between the two respective electron density regions. The simulations involved running the full CTIP model (for equinox, solar maximum conditions), but purposefully allowing only the "E region" and then "F region" components of the neutral wind (in two respective experiments) to be fed into the electrodynamics solver. It must be understood that "doctored" experiments of this kind are undertaken with great care, and the outputs are only used, and discussed, very tentatively. After all, CTIP, and the Earth's real upper atmosphere, are highly "nonlinear" systems and thus "hard" results cannot really be obtained by using techniques of this kind. That said, the results from these runs can still be very instructive and are given in Figure 7. As before, the plot shows the vertical **ExB** drift at 300 km and the magnetic equator, plotted against local time for a geographic longitude of 289°E. The solid line shows the results for the CTIP simulation in which only the E region component of the neutral wind is allowed to contribute to the calculated **ExB** drift. The dotted line shows an identical CTIP simulation, but with only the F region wind allowed to contribute. Figure 7 shows clearly the way in which the thermospheric E and F region dynamos are separately responsible for the various accepted features of the equatorial vertical ion motion. First, it is clear that the prereversal enhancement feature, around 1900 LT, is associated with the wind at F region heights. In addition, Figure 7 shows that in the absence of the E region dynamo effects, the pre reversal enhancement is extremely large, with a maximum velocity of around 100 ms^{-1}. Indeed, it is clear that the E region dynamo is working in opposition to the F region dynamo here, a result which appears generally applicable at all local times (i.e., note the "mirror image" quality of the solid and dotted lines). Figure 7 also shows that it is the E region tidal dynamo which is responsible for the upward **ExB** drift during the daytime (0700 to 1500 LT), with the F region dynamo contributing very little during this time. Finally, as expected, it is the F region dynamo which is responsible for the downward **ExB** motion during nighttime, an effect which is sharply curtailed at dawn (around 0530 LT).

Another set of four CTIP experiments were undertaken to investigate the relative importance of neutral winds at E and F region heights. The four runs were

Table 2. Four CTIP runs

Runcode	wind component fed to electrodynamics	line in Figures 8 and 9
A	Zonal E-region wind	solid line
B	Meridional E-region wind	dotted line
C	Zonal F-region wind	dashed line
D	Meridional F-region wind	dot-dashed line

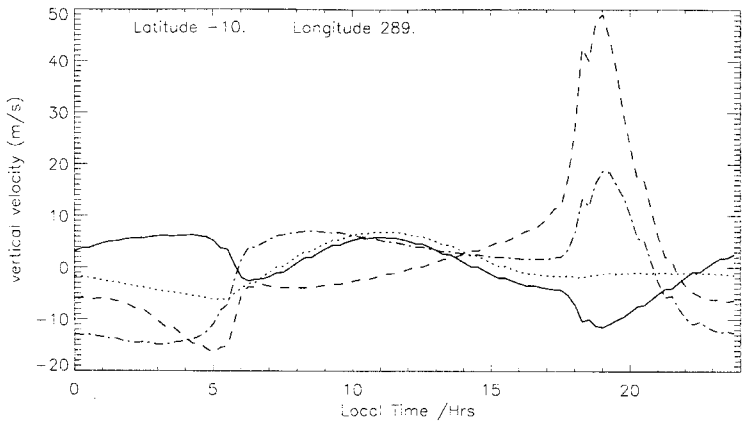

Figure 8. Vertical **ExB** drift velocity plotted against local time for equinox, solar maximum conditions. The lines show results from four CTIP simulations, as given in Table 2.

similar to those discussed in the paragraph above , as plotted in Figure 7 (i.e., equinox, solar maximum conditions). The thermospheric wind, applied to the electrodynamics solver, was defined as either E region (97 to 160 km) or F region (160 to 470 km), as before. The four experiments then involved solving the global electrodynamics with one of four sole wind components, given in Table 2.

The results are plotted in Figure 8 with the four lines as given in Table 2. From Figure 8 it is clear that both the tidally driven zonal and meridional E region winds (solid and dotted lines, respectively) lead to moderate daytime upward motion with a maximum, in these simulations, at around 1100 LT. In addition, the F region meridional wind (dot-dashed line) appears responsible for the "sunrise reversal" in the ion motion (from downward to upward) at around 0530 LT and also for the positive values in the early morning (0600 to 1000 LT). Thus these results show that a combination of both E and F region winds are important in generating upward daytime ion motion, with only the F region zonal component of little importance. Figure 8 also shows clearly that it is the F region zonal wind which is responsible for generating the prereversal enhancement in **ExB** drift around 1900 LT. It is noticeable that the E region zonal wind leads to a downward vertical ion motion at this time (i.e., the negative value of the solid line around 1900 LT). It therefore seems possible that the prereversal enhancement would be of even larger magnitude were it not for the dynamo action of the E region zonal wind. During the nighttime it is the F region dynamo which leads to downward ion motion. In this regard the F region meridional wind appears particularly important, with the dot-dashed line clearly negative between 0000 and 0400 LT.

A similar series of experiments to those documented above (and plotted in Figure 8) were conducted for solar minimum, June solstice, conditions. Again, individual components of the thermospheric wind (zonal E region, meridional F region, etc., as given in Table 2) were used as input to the electrodynamic solver. The tidal forcing used was taken from the values of *Forbes and Vial* [1989], as given in Table 1. Results are shown in Figure 9. Two main points are apparent. First, the large "sunrise enhancement," seen in the June solstice CTIP results in Figures 2 and 3b, is clearly linked to the dynamo

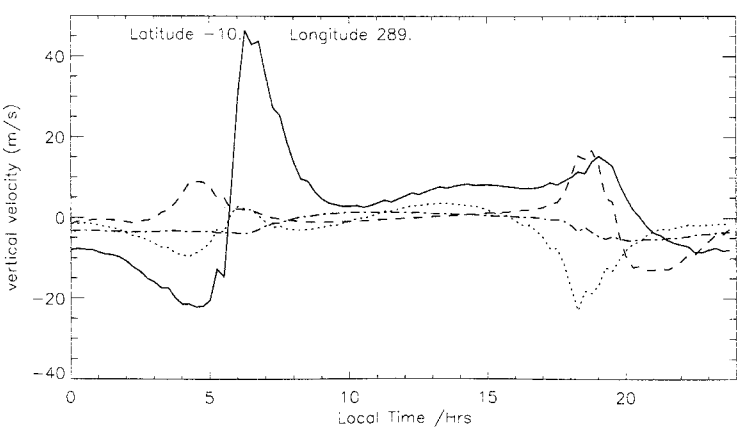

Figure 9. As for Figure 8, but for June solstice, low solar activity conditions. The tidal forcing used is as given in Table 1.

actions of the E region zonal wind (solid line in Figure 9). Second, the prereversal enhancement is related to relatively equal, and moderate, enhancements from the dynamo actions of both the zonal E region and zonal F region winds (solid and dashed lines). The dynamo associated with the meridional E region wind (dotted line) acts in opposition to the enhancement, leading to a greatly diminished prereversal enhancement overall. Interestingly, in this case the meridional F region wind appears to have virtually no effect (dot-dashed line).

6. Conclusions

The simulations outlined in this paper reveal CTIP to be extremely useful as a tool for analyzing, and interpreting, the electrodynamic coupling between the thermosphere and ionosphere at low latitudes. Many of the known features of this coupling are reproduced well by the model and allow us better understanding of the various factors at work from our ability to have access to the many "internal" physical parameters. The model also helps our understanding by allowing "experiments" to be undertaken in which the full system is constrained in some way (e.g., assessing the electrodynamic response to a solitary wind component such as the E region zonal wind). Our results show the importance of lower thermospheric tidal forcing on the daytime vertical ion drift. In particular, it is clear that the semidiurnal tide plays a large role in determining upward ion motion and thus the daytime equatorial ionospheric anomaly. Variablilty within the tidal forcing, such as that observed and discussed on a seasonal and year to year basis by *Goncharenko and Salah* [1998] and on a daily basis by *Salah* [1994] and *Zhou et al.* [1997], will undoubtedly play a role in determining the observed variability within the dayside vertical **ExB** drift, and the distribution of equatorial F region plasma. Our studies show the zonal, eastward, F region wind to be a key factor in the prereversal enhancement during times when this feature is strong (such as equinox, solar maximum). In this regard our results are in agreement with similar studies undertaken recently using the National Center for Atmospheric Research Thermosphere Ionosphere Electrodynamic General Circulation Model (NCAR TIEGCM) [*Fesen et al.*, 2000]. In addition, the role within the E region is noted, particularly the tendency for the E region dynamo to act in opposition to the upward enhancement. Indeed, it may be the case that at times when little enhancement is observed (at certain longitudes and seasons, and particularly for solar minimum) it is dynamo action in the E region which is acting in opposition to the upward motion. Such a conclusion, however, remains tentative and requires further study.

Acknowledgments.

The authors would like to thank Maura Hagan for helpful comments on the original draft of this paper. Computer simulations were carried out on the Miracle supercomputer, at the HiPerSPACE Computing Centre, UCL. The work was supported in the UK by the Particle Physics and Astronomy Research Council and in the United States by the National Science Foundation under grant ATM-981747 and by the National Aeronautics and Space Administration under the Sun-Earth Connections Theory Program and the Supporting Research and Technology Program.

Janet G. Luhmann thanks referees for their assistance in evaluating this paper.

References

Appleton, E. V., Two anomalies in the ionosphere, *Nature*, *157*, 691, 1946.

Bilitza, D., International reference ionosphere 1990, *Rep. 90-22*, Natl. Space Sci. Data Cent., Greenbelt, Md., Nov. 1990.

Chapman, S., and R. S. Lindzen, *Atmospheric Tides*, D. Reidel, Norwell, Mass., 1970.

Chiu, Y. T., An improved phenomenological model of ionospheric density, *J. Atmos. Terr. Phys.*, *37*, 1563, 1975.

Crain, D. J., R. A. Heelis, and G. J. Bailey, Effects of electrical coupling on equatorial ionospheric plasma motions: When is the F region a dominant driver in the low-latitude dynamo?, *J. Geophys. Res.*, *98*, 6033, 1993a.

Crain, D. J., R. A. Heelis, G. J. Bailey, and A.D. Richmond, Low-latitude plasma drifts from a simulation of the global atmospheric dynamo, *J. Geophys. Res.*, *98*, 6039, 1993b.

Du, J., and R. J. Stening, Simulating the ionospheric dynamo, I, Simulation model and flux-tube integrated conductivities, *J. Atmos. Sol. Terr. Phys.*, *61*, 913, 1999a.

Du, J., and R. J. Stening, Simulating the ionospheric dynamo, II, Equatorial electric fields, *J. Atmos. Sol. Terr. Phys.*, *61*, 925, 1999b.

Eccles, J. V., A simple model of low-latitude electric fields, *J. Geophys. Res.*, *103*, 26,699, 1998a.

Eccles, J. V., Modeling investigation of the evening prereversal enhancenment of the zonal electric field in the equatorial ionosphere, *J. Geophys. Res.*, *103*, 26,709, 1998b.

Fesen, C. G., G. Crowley, R. G. Roble, A. D. Richmond, and B. G. Fejer, Simulation of the pre-reversal enhancement in the low-latitude vertical ion drifts, *Geophys. Res. Lett.*, *27*, 1851, 2000.

Forbes, J. M., and F. Vial, Monthly simulations of the solar semidiurnal tide in the mesosphere and lower thermosphere, *J. Atmos Terr. Phys.*, *51*, 649, 1989.

Fuller-Rowell, T. J., A three-dimensional, time-dependant global model of the thermosphere, Ph.D. Thesis, Univ. of London, England, 1981.

Fuller-Rowell, T. J., and D. Rees, A three dimensional time-dependant global model of the thermosphere, *J. Atmos. Sci.*, *37*, 2545, 1980.

Fuller-Rowell, T. J., and D. Rees, Derivation of a conservation equation for mean molecular weight for a two-constituent gas within a three-dimensional time dependent model of the thermosphere, *Planet. Space Sci.*, *31*, 1209, 1983.

Fuller-Rowell, T. J., D. Rees, S. Quegan, R. J. Moffett, and G. J. Bailey, Interactions between neutral thermospheric composition and the polar ionosphere using a coupled ionosphere-thermosphere model, *J. Geophys. Res.*, *92*, 7744, 1987.

Fuller-Rowell, T. J., D. Rees, S. Quegan, R. J. Moffett, M. V. Codrescu, and G. H. Millward, A coupled thermosphere-ionosphere model, CTIM, in *STEP Handbook on Ionospheric Models*, edited by R. W. Schunk, p.217, Utah State Univ., 1996.

Goncharenko, L. P., and J. E. Salah, Climatology and variability of the semidiurnal tide in the lower thermosphere over Millstone Hill, *J. Geophys. Res.*, *103*, 20715, 1998.

Haerendel, G., J. V. Eccles, and S. Cakir, Theory for mod-

eling the equatorial evening ionosphere and the origin of the shear in the horizontal plasma flow, *J. Geophys. Res.*, *97*, 1209, 1992.

Hagan, M. E., J. M. Forbes, and F. Vial, On modeling migrating solar tides, *Geophys. Res. Lett.*, *22*, 893, 1995.

Hagan, M. E., M. D. Burrage, J. M. Forbes, J. Hackney, W. J. Randel, and X. Zhang, GSWM-98: Results for migrating solar tides, *J. Geophys. Res.*, *104*, 6813, 1999.

Hanson, W. B., and R. J. Moffett, Ionization transport effects in the equatorial *F* region, *J. Geophys. Res.*, *71*, 5559, 1966.

Hedin, A. E., Extension of the MSIS thermosphere model into the middle and lower atmosphere, *J. Geophys. Res.*, *96*, 1159, 1991.

Hedin, A. E., et al., Revised global model of thermospheric winds using satellite and ground-based observations, *J. Geophys. Res.*, *96*, 7657, 1991.

Heelis, R. A., P. C. Kendall, R. J. Moffett, D. W. Windle, and H. Rishbeth, Electrical coupling of the *E* and *F* regions and its effect on *F* region drifts and winds, *Planet. Space Sci.*, *22*, 743, 1974.

Kelley, M. C., *The Earth's Ionosphere: Plasma Physics and Electrodynamics*, *Int. Geophys. Ser.*, vol. 43, Academic, San Diego, Calif., 1989.

Millward, G. H., A global model of the Earth's thermosphere, ionosphere and plasmasphere: Theoretical studies of the response to enhanced high-latitude convection, Ph.D. thesis, Univ. of Sheffield, England, 1993.

Millward, G. H., R. J. Moffett, S. Quegan, and T. J. Fuller-Rowell, A coupled ionosphere-thermosphere-plasmasphere model, CTIP, in STEP Handbook on Ionospheric Models, edited by R. W. Schunk, p.239, Utah State Univ., 1996.

Müller-Wodarg, I. C. F., Modelling perturbations propagating through the mesopause into the Earth's upper atmosphere, Ph.D. thesis, Univ. of London, England, 1997.

Müller-Wodarg, I. C. F., A. D. Aylward, and T. J. Fuller-Rowell, Tidal oscillations in the thermosphere: A theoretical investigation of their sources, *J. Atmos. Terr. Phys.*, *63*, 899, 2001.

Namgaladze, A. A., Y. N. Koren'kov, V. V. Klimenko, I. V. Karpov, V. A. Surotkin, and N. M. Naumova, Numerical modeling of the thermosphere-ionosphere-protonosphere system, *J. Atmos. Terr. Phys.*, *53*, 1113, 1991.

Quegan, S., G. J. Bailey, R. J. Moffett, R. A. Heelis, T. J. Fuller-Rowell, D. Rees., and A. W. Spiro, A theoretical study of the distribution of ionization in the high-latitude ionosphere and the plasmasphere: First results on the mid-latitude trough and the light ion trough, *J. Atmos. Terr. Phys.*, *44*, 619, 1982.

Richmond, A. D., Equatorial electrojet, I, Development of a model including winds and instabilities, *J. Atmos. Terr. Phys.*, *35*, 1083, 1973a.

Richmond, A. D., Equatorial electrojet, II, Use of the model to study the equatorial ionosphere, *J. Atmos. Terr. Phys.*, *35*, 1105, 1973b.

Richmond, A. D., and R. G. Roble, Electrodynamic effects of thermospheric winds from the NCAR thermospheric general circulation model, *J. Geophys. Res.*, *92*, 12,365, 1987.

Richmond, A. D., S. Matsushita, and J. D. Tarpley, On the production mechanism of electric currents and fields in the ionosphere, *J. Geophys. Res.*, *81*, 547, 1976.

Richmond, A. D., E. C. Ridley, and R. G. Roble, A thermosphere/ionosphere general circulation model with coupled electrodynamics, *Geophys. Res. Lett.*, *19*, 601, 1992.

Rishbeth, H., The *F* layer dynamo, *Planet. Space Sci.*, *19*, 263, 1971a.

Rishbeth, H., Polarization fields produced by winds in the equatorial region, *Planet. Space Sci.*, *19*, 357, 1971b.

Rishbeth, H., The *F* region dynamo, *J. Atmos. Terr. Phys.*, *43*, 387, 1981.

Rishbeth, H., and O. K. Garriot, *Introduction to Ionospheric Physics*, Academic, San Diego, Calif., 1969.

Scherliess, L., and B. J. Fejer, Radar and satellite global equatorial *F* region vertical drift model, *J. Geophys. Res.*, *104*, 6829, 1999.

Takeda, M., and Y. Yamada, Simulation of ionospheric electric fields and geomagnetic field variation by the ionopsheric dynamo for different solar activity, *Ann. Geophys., Ser. A*, *5*, 429, 1987.

Tarpley, J. D., The ionospheric wind dynamo, II, Solar tides, *Planet. Space Sci.*, *18*, 1091, 1970.

Woodman, R. F., Vertical drift velocities and east-west electric fields at the magnetic equator, *J. Geophys. Res.*, *75*, 6249, 1970.

G. H. Millward, A. D. Aylward, and I. C. F. Müller-Wodarg, Atmospheric Physics Laboratory, Department of Physics and Astronomy, University College London, 67-73 Riding House Street, London, W1P 7PP, UK. (alan@apg.ph.ucl.ac.uk; george@theory.phys.ucl.ac.uk; i.mueller-wodarg@ucl.ac.uk)

T. J. Fuller-Rowell, CIRES, University of Colorado/NOAA, Space Environment Center, 325 Broadway, Boulder, CO 80303. (tim.fuller-rowell@noaa.gov)

R. J. Moffett, Upper Atmosphere Modelling Group, Department of Applied Mathematics, University of Sheffield, Hounsfield Road, Sheffield S3 7RH, UK. (r.moffett@sheffield.ac.uk)

A. D. Richmond, High Altitude Observatory, National Center for Atmospheric Research, P.O. Box 3000, Boulder, CO 80307. (richmond@hao.ucar.edu)

(Received September 6, 2000; revised December 5, 2000; accepted December 5, 2000.)